

Numerical Investigation of LSD Wave Characteristics Using a 1-D Laser-induced Discharge Model

Rei Kawashima¹, Joseph A. Ofosu², Kohei Matsui¹, Toru Shimano², Kimiya Komurasaki¹, Kohei Shimamura³, and Hiroyuki Koizumi²

¹*Dept. of Aeronautics and Astronautics, The University of Tokyo, Bunkyo, Tokyo, 113-8656, Japan*

²*Dept. of Advanced Energy, The University of Tokyo, Kashiwa, Chiba, 277-8561, Japan*

³*Dept. of Engineering Mechanics and Energy, University of Tsukuba, Tsukuba, Ibaraki, 305-8577, Japan*

Abstract

One-dimensional numerical simulation using the reference frame was conducted to investigate the characteristics of the laser-induced ionization wave. The radiative transfer equations for the laser and ultraviolet lights were coupled with the fluid equations for electrons and neutral particles. It was proven that the simulation using the reference frame was useful for the wave-propagation analysis. The simulated ionization wave velocity was on the same order of magnitude as the Chapman-Jouguet velocity. Also, the estimated electron temperature agreed with the experimental result.

Nomenclature

c	:	speed of light
D	:	diffusion coefficient
e	:	elemental charge
h	:	Planck constant
I	:	light intensity
m	:	mass
n	:	number density
P	:	power
S	:	particle source
Z_{eff}	:	effective nuclear charge
ε	:	energy
ε_0	:	vacuum permittivity
λ	:	wavelength
μ	:	mobility
ν	:	frequency
σ	:	cross-section
ω	:	angular frequency
Ω	:	solid angle

Subscript

abs	:	absorption
col	:	collision
e	:	electron
i	:	ion
in	:	inflow
ion	:	ionization
las	:	laser
L	:	left-running UV light
n	:	neutral
photo	:	photoionization
rad	:	radiation
R	:	right-running UV light

1. Introduction

The beamed energy propulsion (BEP) is one of the proposed transportation systems from ground to space. The advantages of the BEP are high specific impulse and high thrust as well as low propulsion weight since onboard propellants are not required. Among the BEP concepts, the applicability of high-power laser has been demonstrated by Myrabo et al. [1], within the experiments using the lightcract. Also, the launch capability and cost of the laser-powered orbital launcher have studied by Katsurayama et al. [2]. It has been proven that a significant

cost reduction is expected by using the laser propulsion.

The thrust force in the laser propulsion is yielded by the high pressure generated in the laser-supported detonation (LSD) process. In the LSD regime, an ionization wave absorbing the laser power travels with the shock wave. The propagation process in the LSD was described by the Raizer's theory [3]. This theory was simply based on the one-dimensional steady-state hydrodynamics conservation laws with heat interaction. However, in some conditions, the propagation velocity predicted by the Chapman-Jouguet condition in the theory did not agree with the measured values [4]. Eventually, it has been suggested that some non-hydrodynamic ionization mechanism are more important than the shock waves.

To account for the non-hydrodynamic ionization mechanism, a hypothesis has been built that the ultraviolet (UV) lights emitted by the plasma behind the shock wave cause photoionization in front of the ionization wave. The assumed processes are as follows: the photoionization by the UV lights provide the seed electrons, and then the main ionization is induced by the avalanche ionization. Recently, a simple analytical model which considered the avalanche ionization and photoionization has been proposed by Shimamura et al. [5]. It was reported that the propagation velocity of the LSD wave predicted by the model agreed with the experimental results. However, this model relies on the electron number densities and electron temperature obtained by the experiments. Therefore, an established model which describes the major characteristics of the discharge has not been proposed.

The objective of this paper is to propose a laser-induced discharge model which considers both of the effects of the avalanche ionization and photoionization. The fundamental assumptions are based on the analytical model proposed in Ref. [5]. To capture the characteristics of the ionization wave, a one-dimensional model using the reference frame fixed to the wavefront is constructed. The effectiveness of the computation using the reference frame and the validity of the model are discussed.

2. 1-D laser-induced discharge model

The major assumptions of the model are as follows:

- (1) A large planar ionization wave is formed perpendicular to the incident laser beam. The properties change only along the direction of the incident laser (x -axis).
- (2) The incident laser energy is absorbed by the inverse Bremsstrahlung (IB) process.
- (3) The laser energy absorbed by electrons is instantaneously consumed in ionization. Thus, the electron energy equation is skipped in the energy conversion process between the laser and ionization.
- (4) Ultraviolet (UV) lights are emitted by the Bremsstrahlung radiation process. The emitted UV lights cause photoionization.
- (5) The ambipolar diffusion is predominant in the electron diffusion process.

The concept of the model using a reference frame is illustrated in Fig. 1. The fundamental equation set for calculating the laser-induced ionization wave consists of the radiative transfer equations (RTEs) and fluid equations. For each equation, a steady state is assumed by using the reference frame fixed to the ionization wave. At the steady state, the speed of moving grid corresponds to the ionization wave velocity.

The first equation is the RTE of the incident laser beam, which is formulated as follows:

$$-\frac{\partial I_{\text{las}}}{\partial x} = -P_{\text{las,abs}}. \quad (1)$$

where I_{las} is the left-running laser intensity. The inverse Bremsstrahlung (IB) absorption is assumed for the absorption process. Hence $P_{\text{las,abs}}$ is expressed as follows:

$$P_{\text{las,abs}} = n_e \sigma_{\text{las,abs}} I_{\text{las}}, \quad (2)$$

where n_e and $\sigma_{\text{las,abs}}$ are the electron number density and absorption cross-section for the laser, respectively. $\sigma_{\text{las,abs}}$ is calculated as follows:

$$\sigma_{\text{las,abs}} = \frac{1}{c \epsilon_0} \frac{e^2}{m_e} \frac{\nu_{\text{col}}}{\omega_{\text{las}}^2 + \nu_{\text{col}}^2}. \quad (3)$$

The electron-neutral scattering collision is assumed for estimating the collision frequency ν_{col} . The angular frequency of the laser ω_{las} is calculated by using the relation $\omega_{\text{las}} = 2\pi c / \lambda_{\text{las}}$.

In addition to the laser beam, the RTEs for the ultraviolet (UV) lights emitted from the plasma are considered. The RTEs for the right- and left-running UV lights are written as follows:

$$\frac{\partial I_{\text{R}}}{\partial x} = P_{\text{R,rad}} - P_{\text{R,abs}}, \quad (4)$$

$$-\frac{\partial I_{\text{L}}}{\partial x} = P_{\text{L,rad}} - P_{\text{L,abs}}, \quad (5)$$

where I_{R} and I_{L} are the right- and left-running UV-light intensities, respectively. The Bremsstrahlung radiation process is assumed for the UV-light radiation. The volumetric power of the continuous plasma radiation per unit

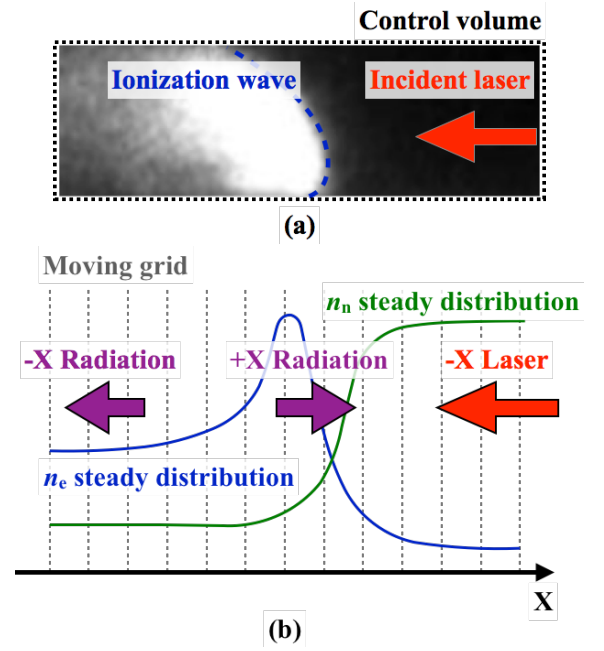


Fig. 1. (a) A self-emission image of the laser-induced discharge. The control volume for the simulation is depicted. (b) The concept of the 1-D laser induced discharge model.

frequency per unit solid angle i_ν is given as follows [5]:

$$i_\nu = 6.3 \times 10^{-53} \frac{Z_{\text{eff}}^2 n_e^2}{\sqrt{e T_e}} \exp\left(-\frac{h\nu}{e T_e}\right), \quad (6)$$

where Z_{eff} is the effective nuclear charge. The UV lights contributing to the photoionization are derived by integrating i_ν with the energy greater than the ionization energy. Further, the radiations included in the right- and left-running lights are estimated by integrating i_ν within the hemisphere, respectively. Thus, $P_{\text{R,rad}}$ and $P_{\text{L,rad}}$ are calculated as follows:

$$P_{\text{R,rad}} = P_{\text{L,rad}} = \int_0^{2\pi} \int_{\epsilon_{\text{ion}}}^{\infty} i_\nu d\epsilon d\Omega, \quad (7)$$

where ϵ_{ion} is the ionization energy. The UV lights are consumed in the photoionization. $P_{\text{R,rad}}$ and $P_{\text{L,rad}}$ are respectively expressed as follows:

$$P_{\text{R,abs}} = -n_n \sigma_{\text{photo}} I_{\text{R}}, \quad (8)$$

$$P_{\text{L,abs}} = -n_n \sigma_{\text{photo}} I_{\text{L}}, \quad (9)$$

where photoionization cross-section σ_{photo} is given by the experimental data.

The electron flow is simply modeled by using the ambipolar diffusion equation. This equation is described in the reference frame moving with the ionization wave velocity. Thus, the equation for the electron flow in the steady state is written as follows:

$$\frac{\partial}{\partial x} \left(-U_{\text{wav}} n_e + D_{\text{amb}} \frac{\partial n_e}{\partial x} \right) = S_{\text{e,col}} + S_{\text{e,photo}}, \quad (10)$$

where U_{wav} and D_{amb} are the ionization wave velocity and ambipolar diffusion coefficient, respectively. $S_{\text{e,col}}$ and $S_{\text{e,photo}}$ are the source of electrons by the collisional ionization and photoionization, respectively. The determination method of U_{wav} is described in Sec. 3.2. D_{amb}

is calculated as follows:

$$D_{\text{amb}} = \frac{\mu_i D_e + \mu_e D_i}{\mu_i + \mu_e}. \quad (11)$$

It is assumed that the laser energy absorbed by electrons is instantaneously consumed in ionization. Hence $S_{e,\text{col}}$ can be expressed as follows:

$$S_{e,\text{col}} = \frac{P_{\text{las,abs}}}{e\varepsilon_{\text{ion}}}. \quad (12)$$

Similarly, $S_{e,\text{photo}}$ is given as follows:

$$S_{e,\text{photo}} = \frac{P_{\text{R,abs}} + P_{\text{L,abs}}}{e\varepsilon_{\text{ion}}}. \quad (13)$$

The assumption of the instantaneous energy conversion between the laser and ionization also gives a clue for estimating the electron temperature. This assumption implies that the electron temperature is adjusted to achieve the relation in Eq. (12). $S_{e,\text{col}}$ can also be expressed by using the electron temperature as follows:

$$S_{e,\text{col}} = n_e \nu_{\text{ion}} = n_e n_n f_{\text{ion}}(T_e), \quad (14)$$

where f_{ion} is the convolution of the ionization collision cross-section and electron thermal velocity, and it is a function of the electron temperature [6]. The data of collisional cross-section is needed in calculating f_{ion} , and it is taken from the experimental data [7]. By combining Eqs. (2), (12), and (14), the electron temperature can be estimated as follows:

$$T_e = f_{\text{ion}}^{-1} \left(\frac{\sigma_{\text{las,abs}} I_{\text{las}}}{n_n} \right). \quad (15)$$

The last equation is the mass conservation equation for neutral particles. It is assumed that the neutral flow is also in the steady-state within the reference frame, and the flow velocity is negligibly small compared to the ionization wave velocity. Hence the mass conservation of neutral particles in the reference frame is formulated as follows:

$$\frac{\partial}{\partial x} (-U_{\text{wav}} n_n) = -S_{e,\text{col}} - S_{e,\text{photo}}. \quad (16)$$

3. Calculation condition and numerical method

3.1 Calculation condition

The physical parameters assumed in this simulation are listed in Table I. The gas species is argon. The information of the collision frequency, laser wavelength, and photoionization cross-section are taken from Ref. [5]. The data of mobilities and diffusion coefficients for ion and electron are taken from Ref. [8].

The calculation condition of the one-dimensional simulation is illustrated in Fig. 2. A small electron number density is set at the upstream boundary to minimize the seed-electron supply from the inflow. Also, a Neumann condition for the electron number density is given at the downstream boundary which satisfies the electron flux conservation. The inflow laser intensity is of the same order of magnitude as the incident laser intensity used in the experiments [5]. The right- and left-running UV-light intensities are set at zero on the left- and right-hand side boundaries, respectively. Lastly, the ambient neutral number density is assumed for the inflow condition.

Table I. Assumed physical parameters in the simulation.

Parameter	Symbol	Value
Gas species	-	Argon
First ionization energy, eV	ε_{ion}	15.76
Collision frequency, s^{-1}	ν_{col}	4.06×10^{12}
Laser wavelength, m	λ_{las}	10.6×10^{-6}
Photoionization cross-section, m^2	σ_{photo}	2.92×10^{-21}
Ion mobility, $\text{m}^2 \text{s}^{-1} \text{V}^{-1}$	μ_i	1.90×10^{-4}
Electron mobility, $\text{m}^2 \text{s}^{-1} \text{V}^{-1}$	μ_e	3.95×10^{-2}
Ion diffusion coefficient, $\text{m}^2 \text{s}^{-1}$	D_i	8.46×10^{-6}
Electron diffusion coefficient, $\text{m}^2 \text{s}^{-1}$	D_e	1.58×10^{-1}
Inflow electron number density, m^{-3}	$n_{e,\text{in}}$	1.0×10^{10}
Inflow laser intensity, W m^{-2}	$I_{\text{las,in}}$	1.0×10^{11}
Inflow neutral number density, m^{-3}	$n_{n,\text{in}}$	2.45×10^{25}

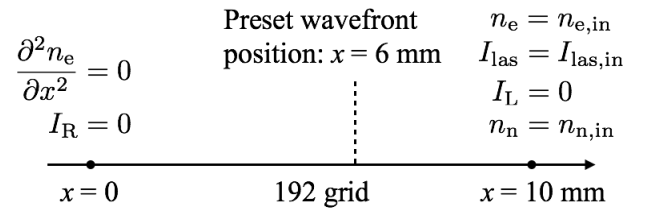


Fig. 2. Calculation condition of the one-dimensional simulation.

The length of the calculation region is 10 mm where a mesh of 192 grids with uniform spacing is used. In the wave-propagation simulation using the reference frame, the wavefront location can be arbitrarily adjusted. In this simulation, the position of the ionization wavefront is preset at $x = 6$ mm. The numerical method to match the wavefront position with the preset position is explained in Sec. 3.2

3.2 Numerical method

The overall calculation flow is illustrated in Fig. 3. The simulation mainly consists of four processes: electron flow calculation, neutral flow calculation, RTE calculation, and wave velocity calculation. These processes are calculated iteratively to derive the steady-state results.

The advection-diffusion equation in Eq. (10) for the electron flow is computed by using an iterative method. The iterative method is constructed by introducing a pseudo-time advancement term as follows:

$$\begin{aligned} \frac{\partial n_e}{\partial t} + \frac{\partial}{\partial x} \left(-U_{\text{wav}} n_e + D_{\text{amb}} \frac{\partial n_e}{\partial x} \right) \\ = S_{e,\text{col}} + S_{e,\text{photo}}. \end{aligned} \quad (17)$$

In the steady state, the pseudo-time advancement term becomes negligibly small and the original equation is satisfied. The second-order upwind method is used for the advection term and the second-order central differencing is used for the diffusion term. To enable a faster convergence, an implicit method using the direct matrix inversion is employed.

The neutral flow in Eq. (16) is also calculated itera-

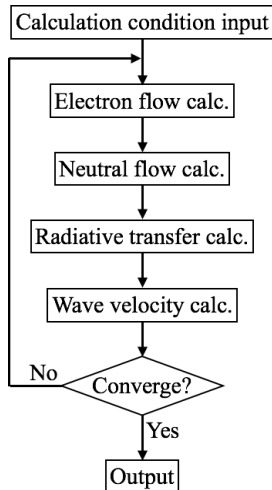


Fig. 3. Calculation flow of the steady-state simulation.

tively as follows:

$$\frac{\partial n_n}{\partial t} + \frac{\partial}{\partial x} (-U_{\text{wav}} n_n) = -S_{e,\text{col}} - S_{e,\text{photo}}. \quad (18)$$

The first-order upwind method is used for discretizing the advection term, and the implicit time advancement is used.

The RTEs for the laser and UV lights are calculated at each pseudo-time step. The space-derivative terms are discretized by using the second-order upwind method. The direct method is used to achieve the instantaneous information conveyance in the RTEs.

This computation utilizes the computational mesh moving with the ionization wave velocity. However, the ionization wave velocity is not known a priori. In some wave-propagation simulations using the reference frame, the wave velocity is found by changing the mesh speed manually [9]. However, it is desired that the wave velocity is automatically determined for efficient analyses. Thus, the uniform ionization wave velocity U_{wav} is calculated by using a pseudo-time advancement as follows:

$$\frac{\partial U_{\text{wav}}}{\partial t} = \alpha (x_{\text{wave}} - x_{\text{wave,preset}}), \quad (19)$$

where x_{wave} and $x_{\text{wave,preset}}$ are the wavefront position and preset wavefront position, respectively. α is an arbitrary coefficient to accelerate the matching between x_{wave} and $x_{\text{wave,preset}}$. By using this equation, the mesh speed is automatically changed to adjust the wavefront location to the preset position.

4. Results and discussion

4.1 Convergence history

First of all, the convergence of the iterative calculation is checked. In this simulation, pseudo-time advancement terms are introduced for electron number density in Eq. (17), neutral number density in Eq. (18), and ionization wave velocity in Eq. (19). Since these time-derivative terms are artificially introduced, they must converge to negligibly small values in the steady state. The magnitude of each pseudo-time advancement term is evaluated

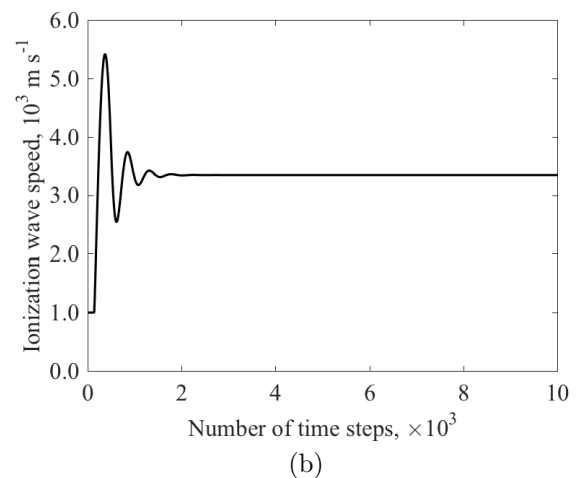
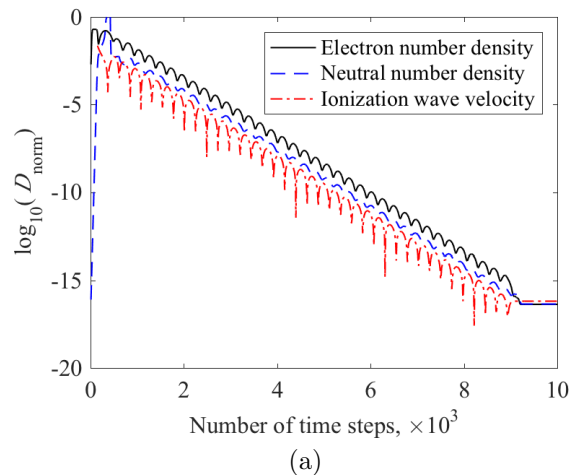


Fig. 4. (a): Convergence histories of the electron number density, neutral number density, and ionization wave velocity. The logarithm of the normalized difference D_{norm} is used for the vertical axis. (b): Iterative history of the ionization wave velocity. $U_{\text{wav}} = 3,340 \text{ m s}^{-1}$ when converged.

by using the normalized difference D_{norm} [10].

Fig. 4 (a) shows the iterative history of the normalized difference for n_e , n_n , and U_{wav} . After about 10^4 iterations, $D_{\text{norm}} \sim 10^{-16}$ is achieved for all the variables. From this result, it is confirmed that all of the pseudo-time advancement terms become negligibly small values in the steady state.

At the steady state, U_{wav} is converged to a specific value. The iterative history of U_{wav} is visualized in Fig. 4 (b). After about 2000 iterations, the U_{wav} is converged to $3,360 \text{ m s}^{-1}$. The Chapman-Jouguet velocity predicted by the Raizer's theory is calculated as $3,400 \text{ m s}^{-1}$, if the specific heat ratio is assumed to be 1.2 [3]. Therefore, the simulated ionization wave velocity is on the same order of magnitude as the Chapman-Jouguet velocity of the LSD wave. From these results, it is concluded that the simulation using the reference frame is successfully implemented, and the ionization wave velocity can be estimated from the simulation.

4.2 Steady-state distribution

After several thousand of time steps, stationary distributions are derived as visualized in Fig. 5. First, the laser

intensity distribution is shown in Fig. 5 (a). A laser-absorption layer exists behind the ionization wavefront and the depth of the layer is approximately 1 mm. The electron temperature is shown in Fig. 5 (b). The electron temperature is uniform and is 1.9 eV. This value agrees with the result of the spectroscopy experiment [5].

However, the obtained electron number density profile is different from the experiments. After the complete absorption of the laser energy, the electron number density exceeds 10^{25} m^{-3} , as presented in Fig. 5 (c). This value is greater than the experimental value by one order of magnitude [5]. Also, in the experiments, it was observed that the electron number density had a peak at about 1 mm behind the ionization wavefront [4]. These discrepancies implies that improvements are required in the physical modeling to reflect the physics of the ionization wave.

5. Conclusion

A one-dimensional numerical simulation is conducted to investigate the characteristics of the ionization wave induced by the laser discharge. The radiative transfer equations for the laser and UV lights are coupled with the fluid equations for electrons and neutral particles. In the simulation, the laser of 100 GW m^{-2} is used for the argon gas in the atmospheric pressure.

It is proven that the simulation using the reference frame is useful for the wave-propagation analysis. All of the pseudo-time advancement terms converge to negligibly small values. The simulated ionization wave velocity is on the same order of magnitude as the Chapman-Jouguet velocity. The estimated electron temperature agrees with the result of spectroscopy experiment. However, a discrepancy is observed between the calculated electron number density and experiments. Improvements are required in the physical modeling to reflect the physics of the ionization wave accurately.

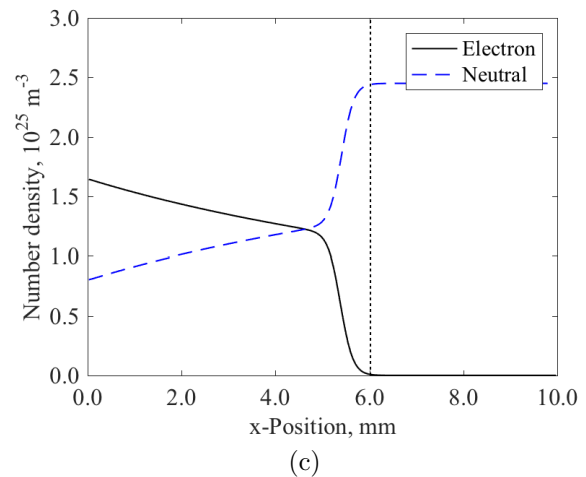
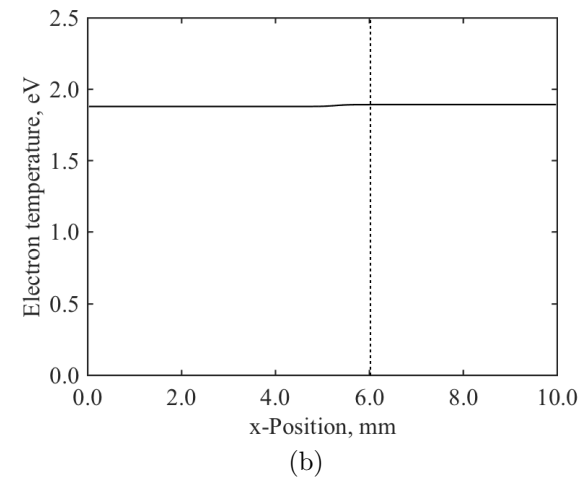
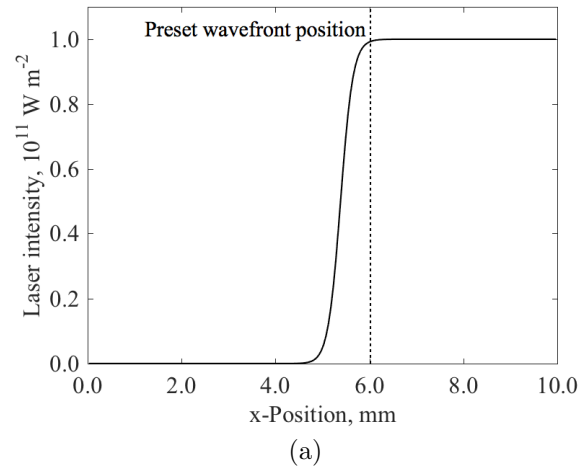


Fig. 5. Steady-state distributions. (a): Laser intensity distribution. (b): Electron temperature distribution. (c): Electron and neutral number density distributions.

- 1) L. Myrabo, D. Messitt, J. Franklin Mead, Ground and flight tests of a laser propelled vehicle, 36th AIAA Aerospace Sciences Meeting and Exhibit, AIAA 98-1001 (1998).
- 2) H. Katsurayama, K. Komurasaki, Y. Arakawa, A preliminary study of pulse-laser powered orbital launcher, *Acta Astronautica* 65 (7–8) (2009) 1032 – 1041.
- 3) Y. P. Raizer, Heating of a gas by a powerful light pulse, *Soviet Physics JETP* 21 (5) (1965) 1508–1519.
- 4) J. A. Ofosu, K. Matsui, K. Komurasaki, K. Shimamura, H. Koizumi, Simulation of lsd wave characteristics in ar and n2 using a 1-d laser-induced discharge model coupled with hydrodynamic relations for laser-propelled thruster studies, 34th International Electric Propulsion Conference, IEPC-2015-464p (2015).
- 5) K. Shimamura, K. Komurasaki, J. A. Ofosu, H. Koizumi, Precursor ionization and propagation velocity of a laser-absorption wave in 1.053 and 10.6- μm wavelengths laser radiation, *IEEE Transactions on Plasma Science* 42 (10) (2014) 3121–3128.
- 6) R. Kawashima, K. Komurasaki, T. Schönherr, H. Koizumi, Hybrid modeling of a hall thruster using hyperbolic system of electron conservation laws, 34th International Electric Propulsion Conference, IEPC-2015-206 (2015).
- 7) M. Hayashi, Bibliography of electron and photon cross sections with atoms and molecules published in the 20th century - argon, NIFS-DATA-72.
- 8) D. P. Lymberopoulos, D. J. Economou, Fluid simulations of

glow discharges: Effect of metastable atoms in argon, *Journal of Applied Physics* 73 (8) (1993) 3668–3679.

- 9) D. E. Paxson, Numerical analysis of a rotating detonation engine in the relative reference frame, NASA/TM-2014-216634.
- 10) R. Kawashima, K. Komurasaki, T. Schönherr, A hyperbolic-equation system approach for magnetized electron fluids in quasi-neutral plasmas, *Journal of Computational Physics* 284 (2015) 59–69.